

Unravelling Water Stability and Electrical Conductivity of 2D Layered Metal-Organic Frameworks in Aqueous Solutions

Mohammad R. Momeni*, Zeyu Zhang, David Dell'Angelo, and Farnaz A. Shakib*

*Department of Chemistry and Environmental Science, New Jersey Institute of Technology,
Newark 07102, NJ United States*

E-mail: momeni@njit.edu,shakib@njit.edu

Abstract

Molecular dynamics simulations combined with periodic electronic structure calculations are performed to decipher structural, thermodynamical and dynamical properties of the interfaced vs. confined water adsorbed in hexagonal 1D channels of the 2D layered electrically conductive $\text{Cu}_3(\text{HHTP})_2$ and $\text{Cu}_3(\text{HTTP})_2$ metal-organic frameworks (HHTP=2,3,6,7,10,11-hexahydroxytriphenylene and HTTP = 2,3,6,7,10,11-hexathiotriphenylene). Comparing water adsorption in bulk vs. slab models of the studied 2D MOFs shows that water is preferentially adsorbed on the framework walls via forming hydrogen bonds to the organic linkers rather than by coordinating to the coordinatively unsaturated open- Cu^{2+} sites. Theory predicts that in $\text{Cu}_3(\text{HTTP})_2$ the van der Waals interactions are stronger which helps the MOF maintain its layered morphology with allowing very little water molecules to diffuse into the interlayer space. Data presented in this work are general and helpful in implementing new strategies for preserving the integrity as well as electrical conductivity of porous materials in aqueous solutions.

Introduction

Conductive π -stacked 2D layered metal-organic frameworks (MOFs)¹ are a new addition to the family of nanoporous materials which offer electrical conductivity^{2–5} in addition to permanent porosity and exceptionally high surface area of conventional 3D MOFs. Crystal structures of 2D MOFs are composed of tetra-coordinated semi-planar metal nodes connected through aromatic linkers creating extended π -conjugated 2D layers in *ab* plane. Stacking of layers *via* $\pi - \pi$ interactions between aromatic triphenylene rings creates parallel, noninterconnected, 1D infinite hexagonal channels along the *c* axis. This architecture provides both *in-plane* and *out-of-plane* electrical conduction as well as directional permeation of electrolyte and target molecules through the conductive material, Figure 1. Owing to this ideal combination, unprecedented breakthroughs are made possible in producing cost-effective semiconductors;^{6,7} supercapacitors;^{8–11} and ion-to-electron transduced chemical sensors.^{12–22} Progress towards these applications calls for a full investigation of stability of π -stacked layered MOFs subject to humidity, and possible hydrolysis of the MOF secondary building unit (SBU), and the effects of these structural transformations on the overall electrical conductivity of the material.

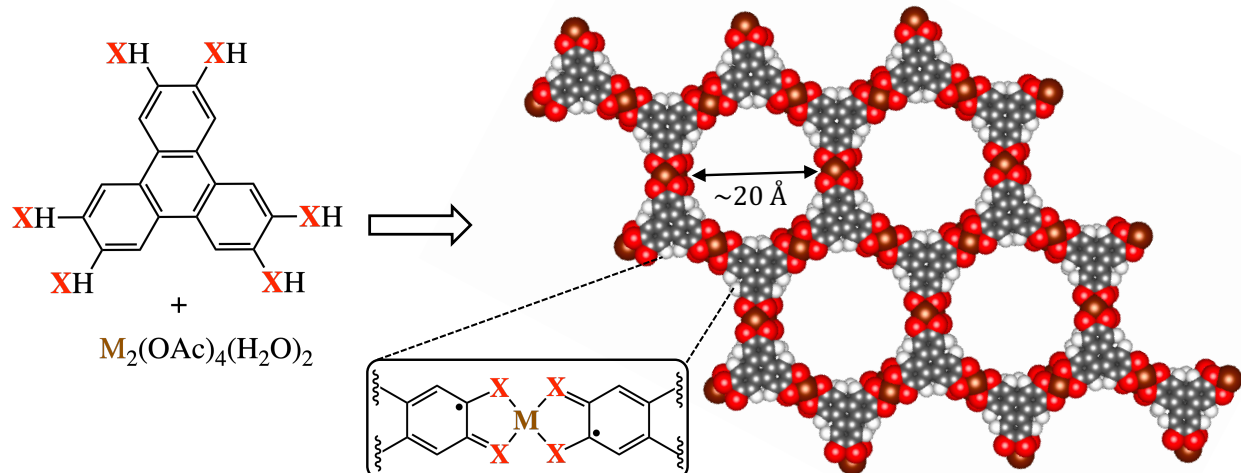


Figure 1: Structure of 2D MOFs. Tritopic linkers and the self-assembled layered architecture along the main 1D channel with $M=\text{Cu}^{2+}$ and $X=\text{O}$ ($\text{Cu}_3(\text{HHTP})_2$) and S ($\text{Cu}_3(\text{HTTP})_2$) in this work.

When it comes to 2D MOFs, little, if not none, experimental data is available on the dynamics of confined water and its adsorption by the framework. There are many important questions to be answered; (i) What are the parameters governing the dynamics of confined water along the 1D channels versus penetration into the interlayer space; (ii) How do the van der Waals interactions reply to the presence of water within the interlayer space; (iii) Will layers be separated due to presence of water or the interlayer water will act as a glue to keep layers together?; (iv) Regardless, how will the presence of water in interlayer space affect the charge mobility between layers and the overall electrical conductivity of the 2D MOFs? and many other such questions.

$\text{Cu}_3(\text{HHTP})_2$ ($\text{HHTP}=2,3,6,7,10,11$ -hexahydroxytriphenylene) is one of the first conductive 2D layered MOFs with metallic behaviour that was synthesized alongside its Co and Ni counterparts in 2012.¹ In our recent study on stability of $\text{Cu}_3(\text{HHTP})_2$ and $\text{Co}_3(\text{HHTP})_2$ in aqueous solutions,²³ we introduced organic linker as an effective player in the dynamics of confined water in 1D channels as well as interlayer space of 2D MOFs. We expect that water is first adsorbed to the 1D channel walls *via* hydrogen bond (HB) formation with organic linkers. The flexible nature of layers and the dynamic HB network finally allows penetration of water molecules within the interlayer space. The penetrated water molecules can then form coordinative bonds with open-metal sites which leads to the increase of interlayer distance and weakening of van der Waals interactions, possibly affecting the overall integrity and electrical conductivity of the layered structure. To verify this hypothesis, here we choose to study dynamics of interface vs. confined water in the slab and bulk models of $\text{Cu}_3(\text{HHTP})_2$ versus $\text{Cu}_3(\text{HTTP})_2$ ($\text{HTTP}=2,3,6,7,10,11$ -hexathiotriphenylene), depicted in Figure 1, as representatives of π -stacked 2D layered MOFs. We will follow the structural, thermodynamical, and dynamical footprints of water in 2D MOFs. Along the path, we will evaluate their effects on the electronic band structure of $\text{Cu}_3(\text{HHTP})_2$ and $\text{Cu}_3(\text{HTTP})_2$ and will differentiate the *in-plane* and *out-of-plane* charge mobility routes. These findings are transferable and applicable to other similar 2D layered nanoporous materials and are useful

in designing more robust water stable materials with desired applications.

Results and discussion

Dynamical picture of the interaction of interface vs. confined water with 2D MOFs

All hydrated systems, both bulk and slab models, were equilibrated in the isothermal-isobaric NPT ensemble for 5 ns. The equilibrated systems are provided in the SI Figure S6 while the final equilibrated slab model of $\text{Cu}_3(\text{HHTP})_2$, with 384 water molecules, is given in Figure 2 as an example. Analysis of water layers in the equilibrated systems reveals five different types of water considering their interactions with the framework. Figure 2 depicts the percentage of water molecules coordinated to one or two open- Cu^{2+} sites (1W_{Cu} and 2W_{Cu}), water molecules hydrogen bonded (HB) to one or two oxygen or sulfur atoms of the linkers (1W_{HB} and 2W_{HB}) and free water molecules (W_F) for both bulk and slab models. Calculated smaller percentage of W_F s in slabs of $\text{Cu}_3(\text{HHTP})_2$ compared to $\text{Cu}_3(\text{HTTP})_2$, regardless of water concentration, clearly shows higher affinity of the former to adsorb water than the latter. Though the metal centers have the same identity in both frameworks but both 1W_{Cu} and 2W_{Cu} are negligible in $\text{Cu}_3(\text{HHTP})_2$ slabs. Confirming our working hypothesis, HB formation with organic linkers are the first step of adsorption. As oxygen atoms of the HHTP linkers form rather stronger HBs with water molecules than sulfur of HTTP, Cu centers in $\text{Cu}_3(\text{HHTP})_2$ are more exposed to the water molecules. Furthermore, the open- Cu^{2+} centers connected to electronegative oxygen atoms in $\text{Cu}_3(\text{HHTP})_2$ are more positively charged compared to the open- Cu^{2+} centers connected to sulfur in $\text{Cu}_3(\text{HTTP})_2$ (SI Tables S1 and S6). The other evidence for our hypothesis is the observed trend in 1W_{Cu} with respect to water concentration that closely follows the trend of 1W_{HB} , Figure 2. The bulk models, more or less, follow the same trends. To illustrate a more informative picture of dynamics of water, we calculated water reorientation relaxation times (τ_2 in ps)

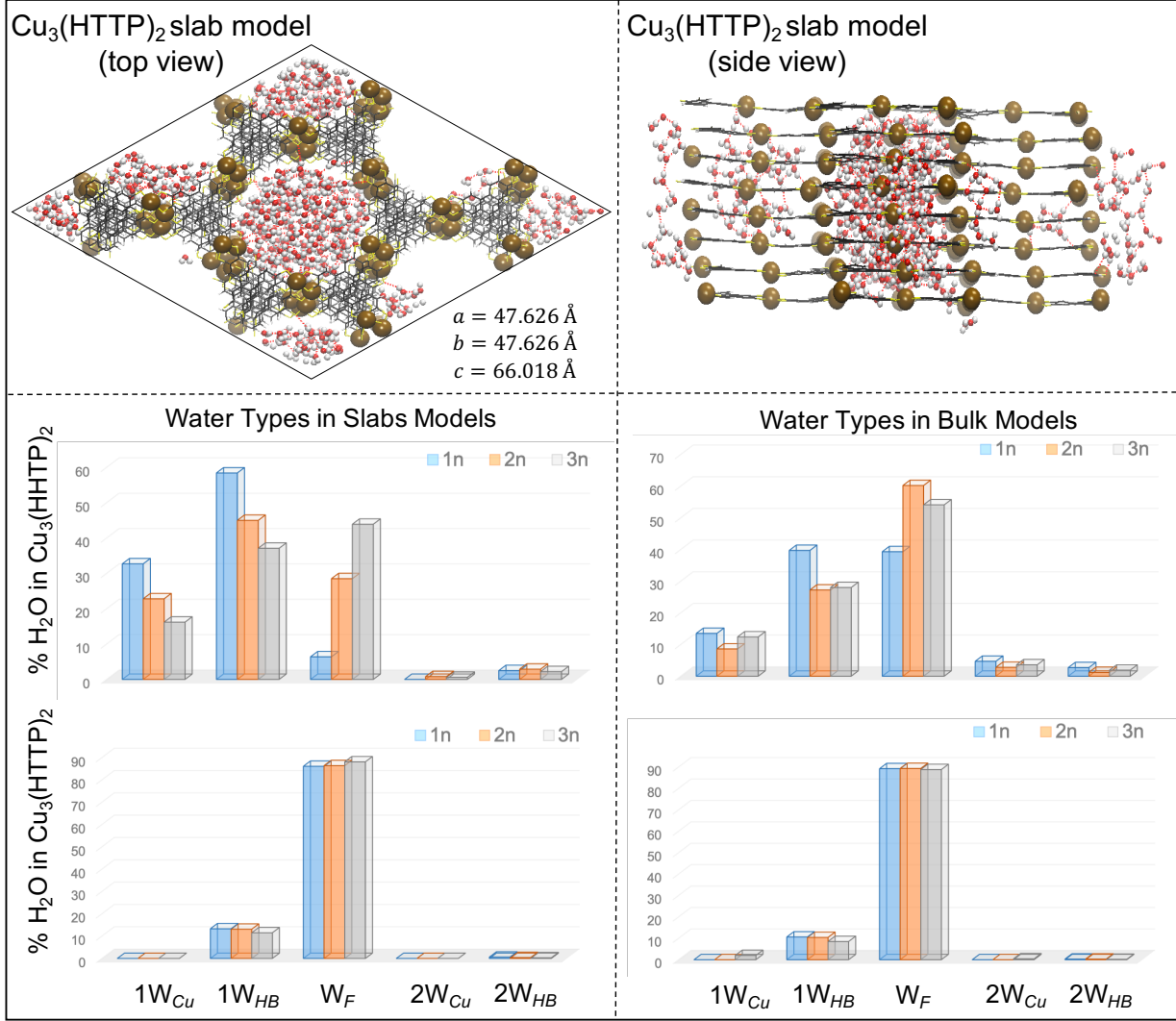


Figure 2: Top: top and side views of representative snapshots for equilibrated slab models of Cu₃(HHTP)₂ with the highest water loading of 384 H₂O and with the equilibrated dimensions of the simulations box given. Calculated percentage different types of water molecules in the slab (left) and bulk (right) models of Cu₃(HHTP)₂ (middle) and Cu₃(HHTP)₂ (bottom) MOFs with different water loadings. *n* refers to the number of Cu²⁺ centers in the unit cell which is equal to 48 in the bulk and 96 in the slab models. Water molecules coordinated to one or two open-Cu²⁺ sites (1W_{Cu} and 2W_{Cu}), hydrogen bonded (HB) to one or two oxygen or sulfur atoms of the linkers (1W_{HB} and 2W_{HB}) as well as free water molecules (W_F) for both bulk and slab models are shown.

and diffusion coefficients along the interlayer space (D_{xy}) and the main 1D channel (D_z) as well as total diffusion coefficients (D_{tot}), see Table 1. We calculated D_{tot} based on the mean

square displacement of the particles²⁴ using the following equation:

$$D = \lim_{t \rightarrow \infty} \frac{1}{6t} \langle (\mathbf{r}(t) - \mathbf{r}(0))^2 \rangle \quad (1)$$

We quantified water reorientation relaxation times in terms of the orientational time correlation functions (TCFs). Then, formulated TCFs in terms of the reorientation of the unit vector $\hat{\mathbf{u}}_{OH}$ that lies along one of the OH bonds of a water molecule:

$$C_{2,OH}(t) = \langle P_2[\hat{\mathbf{u}}_{OH}(0)\hat{\mathbf{u}}_{OH}(t)] \rangle \quad (2)$$

where P_2 is the Legendre polynomial of order 2. The time dependence of the 2nd Legendre polynomial is exponential and can be used to determine orientational relaxation time (τ_2):

$$C_{2,OH}(t) \propto \exp\left(-\frac{t}{\tau_2}\right). \quad (3)$$

Table 1: Calculated water reorientation relaxation time (τ_2 in ps), diffusion coefficients along the xy plane (D_{xy}) and z direction (D_z) as well as total diffusion coefficients (D_{tot}) in Å²·ps⁻¹ for bulk and slab (in parenthesis) models of 2D MOFs with different water loadings. Corresponding experimental values are provided for comparison.

Cu₃(HHTP)₂				
n	τ_2	D_{tot}	D_{xy}	D_z
1H₂O/Cu²⁺	18.8 (59.9)	0.063 (0.030)	0.050 (0.028)	0.089 (0.036)
2H₂O/Cu²⁺	17.2 (47.1)	0.051 (0.031)	0.047 (0.029)	0.059 (0.034)
4H₂O/Cu²⁺	25.4 (30.5)	0.039 (0.036)	0.033 (0.035)	0.050 (0.038)
Cu₃(HTTP)₂				
n	τ_2	D_{tot}	D_{xy}	D_z
1H₂O/Cu²⁺	3.1 (4.4)	0.225 (0.232)	0.149 (0.249)	0.376 (0.199)
2H₂O/Cu²⁺	4.7 (4.7)	0.150 (0.165)	0.111 (0.163)	0.228 (0.167)
4H₂O/Cu²⁺	5.8 (5.3)	0.106 (0.129)	0.095 (0.129)	0.126 (0.129)
Exp. bulk water	1.7–2.6 ^{25–27}	0.229 ²⁸		

Comparison of τ_2 values between either bulk or slab models of Cu₃(HHTP)₂ and Cu₃(HTTP)₂ again shows the free nature of water in the latter with calculated τ_2 values in the range of 3.1–5.8 ps close to that of bulk water, Table 1. In comparison, a range of τ_2 values of 17.2–

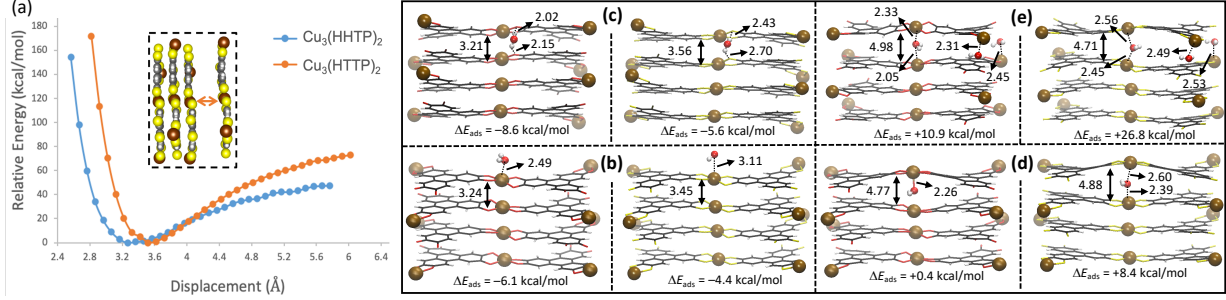


Figure 3: (a) Calculated relative energies (kcal/mol, PBE-D3) for dry slab models of the studied 2D MOFs with minima located at 3.267 Å and 3.519 Å, representing the interlayer distances. To obtain these graphs the top outermost layers are scanned starting from their respective PBE-D3 optimized geometries. (b)-(e) Key bond and interlayer distances (Å, PBE-D3) of different modes of water interacting with the slab models of the Cu₃(HHTP)₂ (left) and Cu₃(HTTP)₂ (right) 2D MOFs.

59.9 ps was found for Cu₃(HHTP)₂. This is in line with the computed D_{tot} values which are 3-8 times higher in Cu₃(HTTP)₂ than Cu₃(HHTP)₂, Table 1. A more informative picture of water dynamics can be obtained from comparison between D_{xy} and D_z since they can shed light on water mobility into the interlayer space vs. the main 1D channel, respectively. In the case of bulk models, D_z is always higher than D_{xy} which shows water molecules cannot move as freely along the xy plane as the z direction. Focusing on bulk Cu₃(HHTP)₂, one can notice a decreasing trend of D_z with increasing water content. This can refer to the adsorption of water molecules by the framework where coordinated water molecules to the metal centers act as nucleation sites and draw more water within the interlayer space, overall reducing their mobility alongside the 1D channel. However, there is also a decreasing trend in D_{xy} with increasing water content. Analysis of MD trajectories, movies are provided as part of SI, shows that as the interlayer space is saturated with water, some are able to penetrate to the nearby channel but due to the high affinity of the framework for adsorbing water they still stay close to the surface. Calculated diffusion coefficients for bulk Cu₃(HTTP)₂ show rather similar trends to those of Cu₃(HHTP)₂ in spite of low affinity of the framework toward water (top panels of Figure 2). In this case, the driving force for the dynamics of water in xy plane can be a network of hydrogen bonded water molecules that move freely

between MOF layers and reaches the nearby channel. Analysis of MD trajectories confirms this hypothesis as the penetrated water molecules in the next channel now form a droplet away from the framework surface. Slab models do not behave as systematically as bulk models since water molecules experience two different environments in the xy direction, one is the interlayer space similar to the bulk model, the other is the interface of the slab with water in the z direction. One certain point that can be drawn from the data in Table 1 regarding slab models is that they generally show smaller D_z values than their counterpart bulk models. The reason is that incoming water molecules toward slab first disperse on the interface where there is plenty of open-metal sites without steric hindrance of an adjacent layer. This overall hinders the ability of the water molecules to enter into the main 1D channels. A combined picture of the dynamics of water in the slab and bulk models shows that in a realistic compact device, incoming water, and any substrate within, would face a physical hindrance to enter the channels of $\text{Cu}_3(\text{HHTP})_2$. After entering the channel, their movement would still be slow due to penetration into the interlayer space. A device made of $\text{Cu}_3(\text{HHTP})_2$ on the other hand would create less physical hindrances for the movement of water, and any other solvated substrates, however, there might be disadvantages of reduced contact time between framework and substrate if performing a catalytic reaction is of interest. In any case, penetration of water within interlayer space is evident regardless of nature of organic linkers. This is expected to lead to an increase in the interlayer distance and possibly weakening of the $\pi - \pi$ and d- π van der Waals interactions. Now, the question is how these structural changes are going to affect the overall stability and electrical conductivity of the layered framework in aqueous solutions?

Thermodynamical footprints of water on structural deformations of 2D MOFs

Our MD simulations discussed in the previous section show that penetration of water molecules within interlayer space can occur regardless of the hydrophilicity or hydrophobicity of the

framework driven by the osmosis effect of the vacant nearby channels. Will this phenomenon result in the separation of layers from each other or water molecules can act as a glue to keep layers together? We turn to quantum mechanical calculations to answer this and similar questions. First, we build a $1 \times 1 \times 2$ slab model comprised of four layers for both $\text{Cu}_3(\text{HHTP})_2$ and $\text{Cu}_3(\text{HTTP})_2$ 2D MOFs suitable for such calculations. To gauge and compare the strength of $\pi - \pi$ interactions in the two systems in the absence of water, the top outermost layer was scanned from $2.567 \text{ \AA} - 5.567 \text{ \AA}$ in $\text{Cu}_3(\text{HHTP})_2$ and from $2.819 \text{ \AA} - 6.019 \text{ \AA}$ in $\text{Cu}_3(\text{HTTP})_2$, Figure 3(a). The minimum of energy occurs at 3.267 \AA for $\text{Cu}_3(\text{HHTP})_2$ and 3.519 \AA for $\text{Cu}_3(\text{HTTP})_2$ representing the interlayer distance in optimized structures. The plateau represent dissociation energy of the outermost layer from the slab which is $\sim 20 \text{ kcal/mol}$ higher for $\text{Cu}_3(\text{HTTP})_2$ than $\text{Cu}_3(\text{HHTP})_2$. This indicates stronger $\pi - \pi$ interactions in the former likely due to the larger atomic radius and polarizability of sulfur compared to oxygen. Next, we use the $1 \times 1 \times 2$ optimized slab models to investigate how water interacts with each system (Figure 3). Panels (b) and (c) of Figure 3 depict two different possible configurations for adsorbing water molecules at the interface of the slab with water, either by coordination to the open-metal site (panel b) or by HB formation with organic linkers (panel c). In each panel, the left figure demonstrates the structural changes in $\text{Cu}_3(\text{HHTP})_2$ due to water adsorption while the right one depicts the corresponding data for $\text{Cu}_3(\text{HTTP})_2$. Consistent with our MD simulations, coordination of water to the open-Cu site in $\text{Cu}_3(\text{HHTP})_2$ is more favorable and is exothermic (as much as 1.7 kcal/mol) than $\text{Cu}_3(\text{HTTP})_2$. As expected, adsorption of water on top of the slab at the interface does not change the interlayer distance considerably. Panel (c) of Figure 3 reveals that adsorption of water by HB formation does not solely occur by the linkers of the outermost layer of the slab. But, the organic linkers of the immediate layer beneath are also sharing the water molecule with the linkers of the outermost layer in both MOFs, Figure 3. Comparison between panels c and b shows that this double HB isomer is 2.5 and 1.2 kcal/mol more stable than the coordinated isomer in $\text{Cu}_3(\text{HHTP})_2$ and $\text{Cu}_3(\text{HTTP})_2$, respectively. This further confirms our classical MD simulation data that HB

formation to the organic linkers is the major form of water adsorption (Figure 2). We also considered the case where the confined water is penetrated within the interlayer space and is simultaneously coordinated to the open Cu site beneath the outermost layer, panels (d) in Figure 3. The penetrated water molecule in the interlayer space is shared between two open-Cu sites which in contrast to two previous isomers is thermodynamically endothermic. The interlayer distance is expanded around 1.4 Å in the area around the coordination site in both MOFs to accommodate the incoming water molecule. This leads to weakening of the stabilizing $\pi - \pi$ interactions. Increasing the number of water molecules to one per Cu²⁺ center in one layer, *i.e.* 3 water molecules, enhances the structural deformation in both MOFs. Now, the interlayer space between two outermost layers is increased across the unit cell, panel (e) in Figure 2. Comparing the results from panel (d) and panel (e) it does not seem probable that water is able to completely saturate the interlayer space and separate the two outermost layers. The PBE-D3 calculated ΔE_{ads} s are 10.5 and 18.4 kcal/mol more endothermic than one water adsorption in Cu₃(HHTP)₂ and Cu₃(HTTP)₂, respectively. On the other hand, the higher ΔE_{ads} of Cu₃(HTTP)₂ than Cu₃(HHTP)₂, +26.8 vs. +10.9 kcal/mol, confirms the less affinity of the former for interacting with water molecules illustrating its higher stability in aqueous solutions.

Electrical conductivity characterization in presence and absence of water

Next, we investigate the effects of water adsorption on electrical conductivity of these materials for applications in aqueous solutions, e.g. as electrodes or electrochemical sensors. In layered 2D materials, the atoms forming the compound are arranged into planes (layers) that are held together by strong in-plane bonds, usually covalent. To form a 3D crystal, the layers are stacked in the out-of-plane direction with weak van der Waals interactions. As a consequence, two different descriptions are usually used for the hopping in a 2D layered semiconductor: through-bond and through-space. The former promotes charge transport via

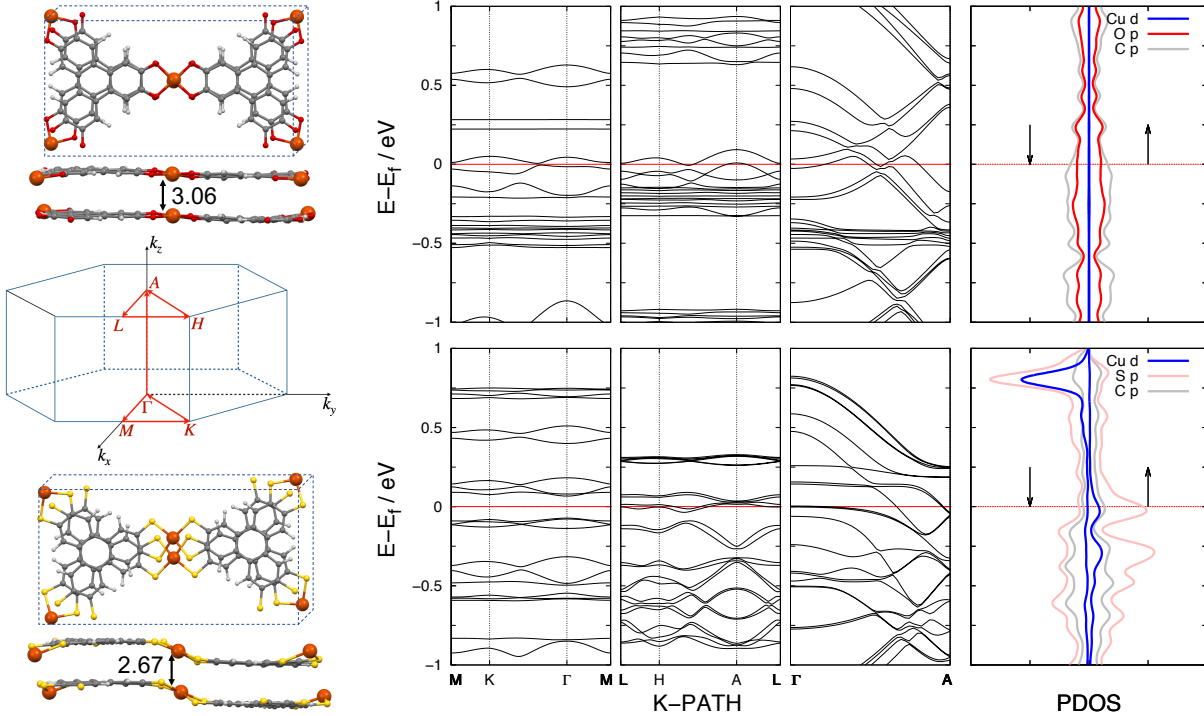


Figure 4: Band structures and projected density of states (PBE+U) of the dry $1 \times 1 \times 1$ $\text{Cu}_3(\text{HHTP})_2$ (top) and $\text{Cu}_3(\text{HTTP})_2$ (bottom) 2D MOFs. The Fermi level is highlighted with a dashed red line with key distances (in Å) given.

favorable spatial and energetic overlap of the metal and ligand orbitals involved in covalent bonding. The latter enables charge transport via non-covalent interactions (such as $\pi - \pi$ stacking).

Dealing with 2D MOFs, the peculiar architecture of the system provides both *in-plane* and *out-of-plane* electrical conductivity. More specifically, as reported by Chen, *et al.*²⁹ they exhibit typical π -conjugated characteristics, since their projected density of states (pDOS) near the Fermi level are almost fully contributed by the p_z orbitals of the ligand as well as the delocalized d orbitals of the transition metal atoms. Yet, this aspect should be contrasted with the role played by metal hybridization. Indeed, it was previously²⁹ shown that Ni^{2+} (d^9) atoms in the $\text{Ni}_3(\text{HITP})_2$ sheet adopt the dsp^2 hybridization to form a square-planar geometry with the organic moieties which allows perfect 2D $\pi - \pi$ conjugation. Conversely, Cu^{2+} (d^9) in $\text{Cu}_3(\text{HITP})_2$ sheet adopts a sp^3 hybridization which results in formation of a rather distorted 2D sheet.

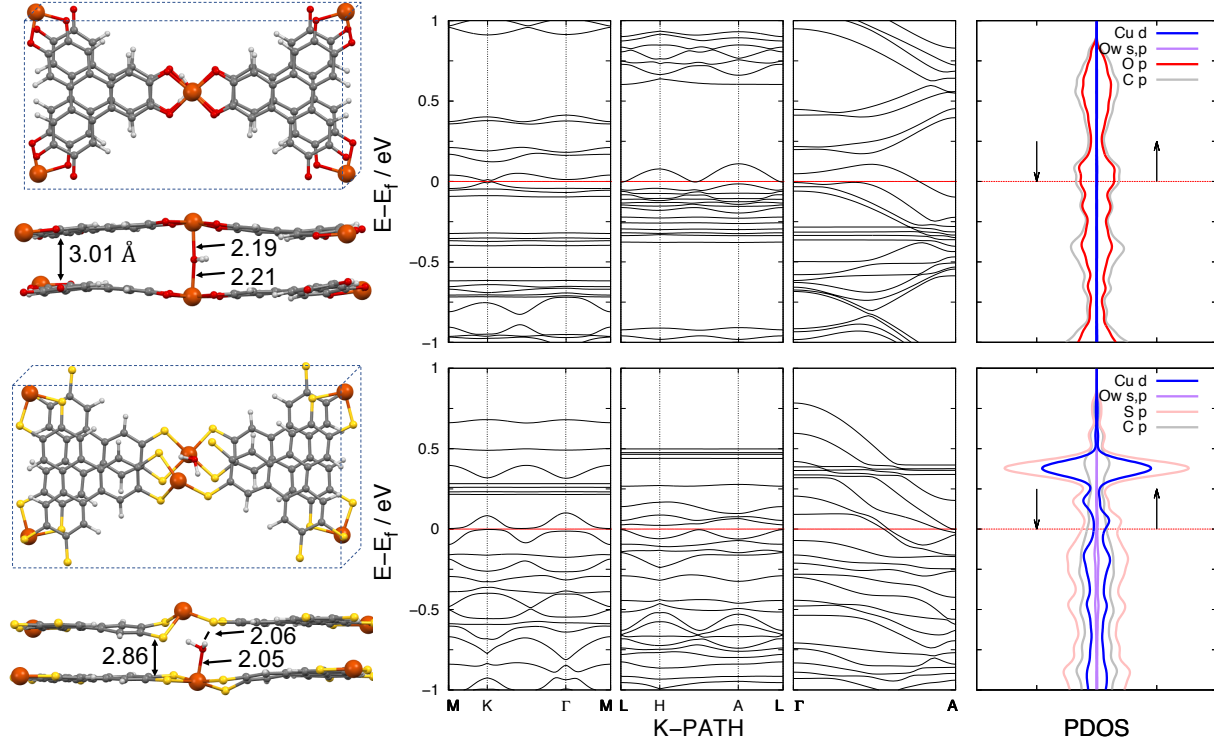


Figure 5: Band structures and projected density of states (PBE+U) of the mono-hydrated $1 \times 1 \times 1$ $\text{Cu}_3(\text{HHTP})_2$ (top) and $\text{Cu}_3(\text{HTTP})_2$ (bottom) 2D MOFs. The Fermi level is highlighted with a dashed red line with key distances (in \AA) given.

The question is how to discern the intra/inter layer contributions in order to account for the intra/inter layer anisotropy in 2D MOFs.³⁰ In intrinsic semiconduction, both thermally and optically excited electrons contribute to the conduction. In the absence of photonic excitation, intrinsic semiconduction takes place at temperatures above 0 K as sufficient thermal activation is required to transfer electrons from the valence band to the conduction band. Then, one may think to monitor the bands crossing at the Fermi level to distinguish the out-of-plane from the in-plane contributions. An alternative way consists of the extrinsic investigation, in which the insertion of impurities in the system may result in deformations (or their lifts) in the intra- and interlayer regions and provide with useful insights dealing with charge transport. In addition, the guest molecules can act as charge carriers themselves, as in the case of ionically conductive MOFs, even if the use of guest molecules in a given material inevitably reduces the porosity.³

From a structural point of view, the two systems under investigation differ in two main aspects (see Figure 4): (a) along the stacking axis, the slight dihedral torsion around the central Cu atom in $\text{Cu}_3(\text{HHTP})_2$ with respect to the main molecular axis, which must be compared to the dihedral torsion *plus* deformation dealing with $\text{Cu}_3(\text{HTTP})_2$; (b) along the main molecular axis, the second layer of $\text{Cu}_3(\text{HTTP})_2$ that slides with respect to the first; by contrast in $\text{Cu}_3(\text{HHTP})_2$ the two layers are eclipsed. Another distinction deals with the ligand nature. Indeed, previous works have shown for instance that the active site for catalytic O_2 reduction in $\text{Ni}_3(\text{HITP})_2$ is not metal-based, as proposed for many transition-metal macrocycles, but rather ligand-based.³¹

Figure 4 displays band diagrams as well as pDOS plots for dry $1 \times 1 \times 1$ unit cells of the $\text{Cu}_3(\text{HHTP})_2$ and $\text{Cu}_3(\text{HTTP})_2$ 2D MOFs. In intralayer regions, the comparison between the band gap along the $\text{MK}\Gamma$ line for $\text{Cu}_3(\text{HTTP})_2$ and the noteworthy semimetallic signature of $\text{Cu}_3(\text{HHTP})_2$ suggests a way to modify the conductive nature of MOFs through the ligand. The overlap between deep valence bands (VBs) (the same goes for conduction bands (CBs)) in $\text{MK}\Gamma$ region of $\text{Cu}_3(\text{HHTP})_2$ as well as the two valleys on each side of the band gap point toward the hopping options along this line. But from the curvature of CB and VB we can infer that along the main molecular axis the mobility is higher for $\text{Cu}_3(\text{HHTP})_2$ than $\text{Cu}_3(\text{HTTP})_2$. $\pi - \pi$ interactions along the z axis do not look affected by slipping deformations and account for relative larger dispersions in the interlayer region.

The pDOS and band diagrams of hydrated $1 \times 1 \times 1$ unit cells of $\text{Cu}_3(\text{HHTP})_2$ and $\text{Cu}_3(\text{HTTP})_2$ are shown in Figure 5. They both disclose a dramatic change in the mobility inserting one water molecule. The impact on mobility is three fold: (a) the interlayer dispersion is reduced, especially in the case of $\text{Cu}_3(\text{HTTP})_2$, in agreement with previous studies³² which shows that the increase of interlayer distance reduces the interlayer hopping and likely affects the mobility in 2D MOFs. (b) Intralayer band gaps open up at the Fermi level for both systems along the LHA line, i.e. the MOF's conductive behaviour deviates from (semi)metallic to semiconductor in this region; instead, in $\text{MK}\Gamma$ region of $\text{Cu}_3(\text{HTTP})_2$ the gap shrinks

moving from dry to hydrated structure. The common feature is the presence of *in*–plane indirect gaps, which means that the conservation of the momentum becomes phonon assisted in this region. The different electron/hole mobilities at the band gap reflect a difference in the electron/hole transition time and then a decrease in the recombination rate, which in turn favours the conductivity. In addition, the valleys in the conduction band suggest charge carrier traps³³ likely triggered by the guest molecule, resulting in photogating enhancement and improved (local) photoconductance.³⁴ (c) Decreasing the ligand affinity, the *in*–plane mobility at the band gap is increased inserting one water molecule, as we can infer from the band curvatures. In the case of Cu₃(HTTP)₂, the presence of the water molecule reduces the contributions of *p*– orbitals at the band gap. As mentioned in (b), band structures add significant insights on how to make the most out of guest molecules by enhancing a conductive behaviour in some specific regions. Finally, deformations as well as interlayer displacements seem to affect only through-bond transfers, and this provide us with a very useful information on how to tailor band gap openings at the Fermi level.

Concluding Remarks

Overall, using a combination of extensive classical molecular dynamics simulations and periodic quantum mechanics calculations the structure, dynamics and thermodynamics of the interfaced vs. confined water in bulk and slab models of 2D MOFs was carefully studied. Theory predicts that water is preferentially adsorbed on the framework walls via hydrogen bond formations with the organic linkers rather than coordination to the coordinatively unsaturated open-Cu²⁺ sites. Our results show that the interlayer van der Waals interactions are stronger in Cu₃(HTTP)₂ compared to its Cu₃(HHTP)₂ analogue which helps the MOF to maintain its layered morphology with allowing very little water molecules to diffuse into the interlayer space. These information on the properties of the interfaced vs. confined water may be employed to taylor 2D MOFs for specific applications, such as catalytic reactions in

operando conditions.

Beyond the influence of water molecules on charge mobility in MOFs, our findings also highlight the potential of both ligands and guest molecules as through-bond descriptors able to discern intra/inter layer anisotropies in 2D MOFs and suggest strategies for designing semiconducting materials. Nonetheless, assessments concerning electrical conductivity require caution, as the latter is influenced by at least four factors, largely in competition with each other. (a) A large energy gap, even if detrimental to light absorption, permits efficient charge separation. Electrons (holes) can follow the conduction (valence) band profile and possibly reach a charge carrier layer, unless (b) they encounter on their way phonons or impurities which in turn (c) may generate charge transport traps that enhance the (local) conductance (i.e., decreasing the resistance of the material). This does not necessarily translate into an increase of the current, as the latter depends on (d) the recombination rate between valleys on the opposite sides of the band gap. For instance, in hydrated Cu₃(HTTP)₂ the opposite valleys exhibit different curvatures and then different mobilities, so one may reasonably expect a decrease in the recombination rate which is beneficial to the charge transport. Yet the band gap shrinks after insertion of one water molecule so it is difficult to argue which of the two factors may prevail. Therefore, the discussion of this intricate issue would deserve, a thorough quantitative analysis through calculations of effective masses and mobilities, a formalism able to take these four factors into account on equal footing. Suggestions for improving charge transport in 2D MOFs may rely on purely chemical intuition, for instance by increasing the molecular overlaps, i.e. optimizing the crystal packing (through pressure or strain). Further thickness reduction to a small number of layers induces quantum confinement in the vertical direction, which has a strong impact on the bandgap of the material. Or by increasing the intermolecular vibration frequency by tightening the intermolecular bonds or multi-valley schemes nearby the Fermi level. Studies in these directions are currently underway in our group.

Computational Methods

A summary of our theoretical methodology is provided below with more details given in the Supporting Information (SI).

Classical molecular dynamics simulations

Classical molecular dynamics (MD) simulations for dry MOFs were initiated from the hexagonal ($\alpha = \beta = 90^\circ$, $\gamma = 120^\circ$, $a = b = 46.470$ Å, and $c = 13.555$ Å) PBE-D3 minimized tetra-layered $2 \times 2 \times 2$ supercell of the bulk $\text{Cu}_3(\text{HHTP})_2$ and $\text{Cu}_3(\text{HTTP})_2$ MOFs (comprised of 1008 atoms in total and 48 metal centers) using DL_POLY_2 package.³⁵ Force field parameters for transition metals involved in SBUs of our 2D MOFs do not exist in Generic force fields such as generalized amber force field (GAFF).³⁶ The first step for generating these parameters is to create a reliable training set of SBUs at *ab initio* level. Starting from the only experimentally available crystallographic data, for $\text{Co}_3(\text{HHTP})_2$,¹ we built a $2 \times 2 \times 2$ super cell for the dry MOF by removing hydrolyzed layers, and all chemisorbed water molecules, replacing Co atoms with Cu and adjusting the interlayer distances to ~ 4 Å. Both cell vectors and atomic positions of this supercell were then minimized with periodic boundary conditions using the Perdew–Burke–Ernzenhof (PBE)³⁷ density functional with damped D3 dispersion correction³⁸ in CP2K version 5.1.³⁹ For creating the training sets, reduced cluster models comprised of a single Cu center and two truncated linkers were cut from the optimized crystal structures (see SI Figure S1). The central metal atoms were then displaced by 0.02 Å from -0.04 Å to +0.04 Å along the x , y and z dimensions (creating a total of 125 configurations). All electronic energies for this training set were calculated using the $\omega\text{B97M-v}$ ⁴⁰ density functional and the def2-TZVP basis set as implemented in QCHEM version 5.2.⁴¹ To fit force field parameters to this *ab initio* training set, Morse potential was used for all coordinative Cu–O and Cu–S bonds while Harmonic potential was employed for the rest. David Carroll's genetic algorithm⁴² was used for fitting all bonded

interactions involving the Cu²⁺ transition metal centers, including bonds, angles, and dihedrals, while all parameters related to the intramolecular interactions present in the organic linkers were taken from GAFF without further modification. The non-bonded parameters concerning transition metal sites include electrostatic as well as van der Waals interactions. To account for the former, we computed atomic charges at the ω B97X-d/def2-TZVP level⁴⁰ using the CHELPG scheme which fits all atomic charges to represent molecular electrostatic potential.⁴³ For the latter, Lennard-Jones parameters of Cu²⁺ were taken from the Universal Force Field (UFF).⁴⁴ More details are given in the SI section S1 as well as validation of the developed force fields are provided in SI section S2. The complete list of the bonded and non-bonded parameters for Cu₃(HHTP)₂ and Cu₃(HTTP)₂ MOFs are given in SI Tables S1-S5 and Tables S6-S10, respectively. A second 2D slab model comprised of eight layers and 2016 atoms was built for both systems to compare the properties of slab and bulk in water adsorption and dissolution. A vacuum space of 40 Å was added to the *c* vector of the slab models. Each system was equilibrated for 5 ns in the isothermal-isobaric NPT ensemble with a time step of 0.2 fs at 293 K temperature and 1 atm pressure, the experimental conditions at which the original 2D MOFs were synthesized,¹ allowing the simulation box to vary. The constant total energy of the systems, with less than 1 kcal/mol fluctuation confirms that 5 ns is indeed enough in order to reach an equilibrated stage. In each 1D channel of our 2×2×2 supercells, there are *n* = 24 open metal sites that are exposed to confined water molecules. Therefore, to study dynamics of confined water in the bulk models, we placed 2*n* = 48, 4*n* = 96 and 8*n* = 192 water molecules in a sphere centered at the middle of the 1D channel of the dry MOF using PACKMOL⁴⁵ code. For the slab models, a layer of water was placed in the vacuum above the slab ~5 Å away from the surface. The equations of motion were propagated according to the velocity-Verlet algorithm. The temperature was kept constant using a Nosé-Hoover chain comprised of four thermostats.⁴⁶ To model water molecules, we use the flexible 4-site qTIP4P/F⁴⁷ quantum water potential which has been shown to be successful in reproducing a diverse number of static and dynamical properties of

water including melting point, diffusion coefficients and IR spectrum. Dynamical properties are calculated from the average of 10 independent 50 ps NVE simulations. These trajectories were run from 10 different initial configurations obtained from 10 ps NVT trajectories that followed the NPT simulations. The final snapshots of these NVT trajectories were then used as initial configurations for 50 ps NVE simulations ensuring that different starting configurations initiate independent NVE trajectories.

Electronic structure calculations

The PBE³⁷ exchange-correlation functional corrected by the DFT-D3 method of Grimme³⁸ as implemented in Vienna Ab Initio Simulation Package (VASP)^{48–51} was used to calculate the band structure and density of states. Hubbard U corrections where U parameter is set to 10.4 eV, suggested by Gregory et al,⁵² are included to treat 3d states of the Cu transition metals.^{53–55} Interactions between electrons and ions were described by Projector Augmented Wave (PAW) potentials^{56,57} with energy cutoff set to 500 eV. Gaussian smearing was adopted in all calculations with a smearing width of 0.05 eV. The convergence criteria were 10^{-5} for self consistent field calculations and 10^{-6} for electronic property calculations. A k -point mesh in the Monkhorst–Pack scheme of $2\times 2\times 6$ was used in the SCF part and twice denser in following calculations. Spin polarized calculations (collinear) were performed for all systems.

Supporting Information Available

Details of our classical MD simulations and quantum mechanical calculations.

Acknowledgement

This work is supported by start-up fund from NJIT and used the Extreme Science and Engineering Discovery Environment (XSEDE) which is supported by NSF grant numbers CHE200007 and CHE200008. This research has been (partially) enabled by the use of computing resources provided by Kong HPC center at NJIT.

References

- (1) Hmadeh, M. et al. New porous crystals of extended metal-catecholates. *Chem. Mater.* **2012**, *24*, 3511–3513.
- (2) Huang, X.; Sheng, P.; Tu, Z.; Zhang, F.; Wang, J.; Geng, H.; Zou, Y.; Di, C.-A.; Yi, Y.; Sun, Y.; Zhu, D. Two-dimensional π -d conjugated coordination polymer with extremely high electrical conductivity and ambipolar transport behavior. *Nat. Commun.* **2015**, *6*, 7408.
- (3) Sun, L.; Campbell, M.; Dincă, M. Electrically conductive porous metal-organic frameworks. *Angew. Chem., Int. Ed.* **2016**, *55*, 3566–3579.
- (4) Clough, A.; Skelton, J.; Downes, C.; de la Rosa, A.; Yoo, J.; Walsh, A.; Melot, B.; Marinescu, S. Metallic conductivity in a two-dimensional cobalt dithiolene metal-organic framework. *J. Am. Chem. Soc.* **2017**, *139*, 10863–10867.
- (5) Dou, J.-H.; Sun, L.; Ge, Y.; Li, W.; Hendon, C.; Li, J.; Gul, S.; Yano, J.; Stach, E.; Dincă, M. Signature of Metallic Behavior in the Metal-Organic Frameworks $M_3(\text{Hexaiminobenzene})_2$ ($M = \text{Ni}, \text{Cu}$). *J. Am. Chem. Soc.* **2017**, *139*, 13608–13611.
- (6) Sheberla, D.; Sun, L.; Blood-Forsythe, M.; Er, S.; Wade, C.; Brozek, C.; Aspuru-Guzik, A.; Dincă, M. High electrical conductivity in $\text{Ni}_3(2,3,6,7,10,11$ -

- hexaiminotriphenylene)₂, a semiconducting metal-organic graphene analogue. *J. Am. Chem. Soc.* **2014**, *136*, 8859–8862.
- (7) Wu, G.; Huang, J.; Zang, Y.; He, J.; Xu, G. Porous field-effect transistors based on a semiconductive metal-organic framework. *J. Am. Chem. Soc.* **2017**, *139*, 1360–1363.
- (8) Sheberla, D.; Bachman, J.; Elias, J.; Sun, C.-J.; Shao-Horn, Y.; Dincă, M. Conductive MOF electrodes for stable supercapacitors with high areal capacitance. *Nat. Mater.* **2016**, *16*, 220–224.
- (9) Li, W.-H.; Ding, K.; Tian, H.-R.; Yao, M.-S.; Nath, B.; Deng, W.-H.; Wang, Y.; Xu, G. Conductive metal-organic framework nanowire array electrodes for high-performance solid-state super-capacitors. *Adv. Funct. Mater.* **2017**, *27*, 1702067.
- (10) Sheberla, D.; Bachman, J.; Elias, J.; Sun, C.; Shao-Horn, Y.; M., D. Conductive MOF electrodes for stable supercapacitors with high areal capacitance. *Nat. Mater.* **2017**, *16*, 220–224.
- (11) Feng, D. et al. Robust and conductive two-dimensional metal-organic frameworks with exceptionally high volumetric and areal capacitance. *Nat. Energy* **2018**, *3*, 30–36.
- (12) Clough, A.; Yoo, J.; Mecklenburg, M.; Marinescu, S. Two-dimensional metal-organic surfaces for efficient hydrogen evolution from water. *J. Am. Chem. Soc.* **2015**, *137*, 118–121.
- (13) Dong, R.; Pfeffermann, M.; Liang, H.; Zheng, Z.; Zhu, X.; Zhang, J.; Feng, X. Large-area, free-standing, two-dimensional supramolecular polymer single-layer sheets for highly efficient electrocatalytic hydrogen evolution. *Angew. Chem., Int. Ed.* **2015**, *54*, 12058–12063.
- (14) Miner, E.; Fukushima, T.; Sheberla, D.; Sun, L.; Surendranath, Y.; Dincă, M. Electro-

- chemical oxygen reduction catalysed by Ni₃(hexaiminotriphenylene)₂. *Nat. Commun.* **2016**, *7*, 10942.
- (15) Huang, X.; Yao, H.; Cui, Y.; Hao, W.; Zhu, J.; Xu, W.; Zhu, D. Conductive copper benzenehexathiol coordination polymer as a hydrogen evolution catalyst. *ACS Appl. Mater. Interfaces* **2017**, *9*, 40752–40759.
- (16) Sun, X.; Wu, K.-H.; Sakamoto, R.; Kusamoto, T.; Maeda, H.; Ni, X.; Jiang, W.; Liu, F.; Sasaki, S.; Masunaga, H.; Nishihara, H. Bis(aminothiolato)nickel nanosheet as a redox switch for conductivity and an electrocatalyst for the hydrogen evolution reaction. *Chem. Sci.* **2017**, *8*, 8078–8085.
- (17) Mendecki, L.; Ko, M.; Zhang, X.; Meng, Z.; Mirica, K. Porous scaffolds for electrochemically controlled reversible capture and release of ethylene. *J. Am. Chem. Soc.* **2017**, *139*, 17229–17232.
- (18) Yao, M.; Lv, X.; Fu, Z.; Li, W.; Deng, W.; Wu, G.; Xu, G. Layer-by-layer assembled conductive metal-organic framework nanofilms for room-temperature chemiresistive sensing. *Angew. Chem., Int. Ed.* **2017**, *56*, 16510–16514.
- (19) Mendecki, L.; Mirica, K. Conductive metal-organic frameworks as ion-to-electron transducers in potentiometric sensors. *ACS Appl. Mater. Interfaces* **2018**, *10*, 19248–19257.
- (20) Jia, H.; Yao, Y.; Zhao, J.; Gao, Y.; Luo, Z.; Du, P. Novel two-dimensional nickel phthalocyanine-based metal-organic framework for highly efficient water oxidation catalysis. *J. Mater. Chem. A* **2018**, *6*, 1188–1195.
- (21) Downes, C.; Clough, A.; Chen, K.; Yoo, J.; Marinescu, S. Evaluation of the H₂ evolving activity of benzenehexathiolate coordination frameworks and the effect of film thickness on H₂ production. *ACS Appl. Mater. Interfaces* **2018**, *10*, 1719–1727.

- (22) Meng, Z.; Aykanat, A.; Mirica, K. Welding metallophthalocyanines into bimetallic molecular meshes for ultra-sensitive, low-power chemiresistive detection of gases. *J. Am. Chem. Soc.* **2019**, *141*, 2046–2053.
- (23) Shi, Y.; Momeni, M. R.; Chen, Y.-J.; Zhang, Z.; Shakib, F. A. Water-Induced Structural Transformations in Flexible Two-Dimensional Layered Conductive Metal–Organic Frameworks. *Chem. Mater.* **2020**, DOI: 10.1021/acs.chemmater.0c03331.
- (24) Nitzan, A. *Chemical Dynamics in Condensed Phases: Relaxation, Transfer, and Reactions in Condensed Molecular Systems*; Oxford University Press, 2006.
- (25) Winkler, K.; Lindner, J.; Bürsing, H.; Vöhringer, P. Ultrafast Raman-induced Kerr-effect of water: Single molecule versus collective motions. *J. Chem. Phys.* **2000**, *113*, 4674.
- (26) Lawrence, C. P.; Skinner, J. L. Vibrational spectroscopy of HOD in liquid D₂O. III. Spectral diffusion, and hydrogen-bonding and rotational dynamics. *J. Chem. Phys.* **2003**, *118*, 264.
- (27) Rezus, Y. L. A.; Bakker, H. J. On the orientational relaxation of HDO in liquid water. *J. Chem. Phys.* **2005**, *123*, 114502.
- (28) Krynicki, K.; Green, C. D.; Sawyer, D. W. Pressure and temperature dependence of self-diffusion in water. *Faraday Discuss.* **1978**, *66*, 199.
- (29) Chen, S.; Dai, J.; Zeng, X. Metal-organic Kagome lattices M₃(2,3,6,7,10,11-hexamiminotriphenylene)₂ (M = Ni and Cu): from semiconducting to metallic by metal substitution. *Phys. Chem. Chem. Phys.* **2015**, *17*, 5954–5958.
- (30) Wang, M. et al. Unveiling Electronic Properties in Metal–Phthalocyanine-Based Pyrazine-Linked Conjugated Two-Dimensional Covalent Organic Frameworks. *J. Am. Chem. Soc.* **2019**, *141*, 16810–16816.

- (31) Miner, E. M.; Gul, S.; Ricke, N. D.; Pastor, E.; Yano, J.; Yachandra, V. K.; Van Voorhis, T.; Dincă, M. Mechanistic Evidence for Ligand-Centered Electrocatalytic Oxygen Reduction with the Conductive MOF $\text{Ni}_3(\text{hexaiminotriphenylene})_2$. *ACS Cat.* **2017**, *7*, 7726–7731.
- (32) Foster, M.; Sohlberg, K.; Spataru, C.; Allendorf, M. Proposed modification of the graphene analogue $\text{Ni}_3(\text{HITP})_2$ to yield a semiconducting material. *J. Phys. Chem. C* **2016**, *120*, 15001–15008.
- (33) Haneef, H. F.; Zeidell, A. M.; Jurchescu, O. D. Charge carrier traps in organic semiconductors: a review on the underlying physics and impact on electronic devices. *J. Mater. Chem. C* **2020**, *8*, 759–787.
- (34) Masurkar, A.; Kymmissis, I. Photocurrent measurements of pentacene-based devices. *App. Phys. Rev.* **2015**, *2*, 031101.
- (35) Smith, T., W.; Forester DL POLY 2.0: A general-purpose parallel molecular dynamics simulation package. *J. Mol. Graph.* **1996**, *14*, 136–141.
- (36) Wang, J.; Wolf, R. M.; Caldwell, J. W.; Kollman, P. A.; Case, D. A. Development and testing of a general amber force field. *J. Computat. Chem.* **2004**, *25*, 1157–1174.
- (37) Perdew, J. P.; Burke, K.; Ernzerhof, M. Generalized Gradient Approximation Made Simple. *Phys. Rev. Lett.* **1996**, *77*, 3865–3868.
- (38) Grimme, S.; Antony, J.; Ehrlich, S.; Krieg, H. A consistent and accurate ab initio parametrization of density functional dispersion correction (DFT-D) for the 94 elements H-Pu. *J. Chem. Phys.* **2010**, *132*, 154104.
- (39) Hutter, J.; Iannuzzi, M.; Schiffmann, F.; VandeVondele, J. cp2k: atomistic simulations of condensed matter systems. *WIREs Comput. Mol. Sci.* **2014**, *4*, 15–25.

- (40) Mardirossian, N.; Head-Gordon, M. ω B97M-V: A combinatorially optimized, range-separated hybrid, meta-GGA density functional with VV10 nonlocal correlation. *J. Chem. Phys.* **2016**, *144*, 214110.
- (41) Shao, Y.; Gan, Z.; Epifanovsky, E.; Gilbert, A. T.; Wormit, M.; Kussmann, J.; Lange, A. W.; Behn, A.; Deng, J.; Feng, X., et al. Advances in molecular quantum chemistry contained in the Q-Chem 4 program package. *Mol. Phys.* **2015**, *113*, 184–215.
- (42) Goldberg, D. *Genetic Algorithms in Search, Optimization and Machine Learning*; Addison-Wesley, 1989.
- (43) Breneman, C. M.; Wiberg, K. B. Determining atom-centered monopoles from molecular electrostatic potentials. The need for high sampling density in formamide conformational analysis. *J. Comput. Chem.* **1990**, *11*, 361–373.
- (44) Rappe, A. K.; Casewit, C. J.; Colwell, K. S.; III, W. A. G.; Skiff, W. M. UFF, a full periodic table force field for molecular mechanics and molecular dynamics simulations. *J. Am. Chem. Soc.* **1992**, *114*, 10024–10035.
- (45) Martínez, L.; Andrade, R.; Birgin, E. G.; Martínez, J. M. PACKMOL: A package for building initial configurations for molecular dynamics simulations. *J. Comput. Chem.* **2009**, *30*, 2157–2164.
- (46) Tuckerman, M. E. *Statistical mechanics: Theory and molecular simulation*; (Oxford University Press, 2010.
- (47) Habershon, S.; Markland, T. E.; Manolopoulos, D. E. Competing quantum effects in the dynamics of a flexible water model. *J. Chem. Phys.* **2009**, *131*, 024501.
- (48) Kresse, G.; Hafner, J. Ab initio molecular dynamics for liquid metals. *Phys. Rev. B* **1993**, *47*, 558–561.

- (49) Kresse, G.; Hafner, J. Ab initio molecular-dynamics simulation of the liquid-metal–amorphous-semiconductor transition in germanium. *Phys. Rev. B* **1994**, *49*, 14251–14269.
- (50) Kresse, G.; Furthmüller, J. Efficiency of ab-initio total energy calculations for metals and semiconductors using a plane-wave basis set. *Comput. Mater. Sci.* **1996**, *6*, 15 – 50.
- (51) Kresse, G.; Furthmüller, J. Efficient iterative schemes for ab initio total-energy calculations using a plane-wave basis set. *Phys. Rev. B* **1996**, *54*, 11169–11186.
- (52) Mann, G. W.; Lee, K.; Cococcioni, M.; Smit, B.; Neaton, J. B. First-principles Hubbard U approach for small molecule binding in metal-organic frameworks. *J. Chem. Phys.* **2016**, *144*, 174104.
- (53) Anisimov, V. I.; Zaanen, J.; Andersen, O. K. Band theory and Mott insulators: Hubbard U instead of Stoner I. *Phys. Rev. B* **1991**, *44*, 943–954.
- (54) Anisimov, V. I.; Aryasetiawan, F.; Lichtenstein, A. I. First-principles calculations of the electronic structure and spectra of strongly correlated systems: The LDA+U method. *J. Phys. Condens. Matter.* **1997**, *9*, 767–808.
- (55) Himmetoglu, B.; Floris, A.; de Gironcoli, S.; Cococcioni, M. Hubbard-corrected DFT energy functionals: The LDA+U description of correlated systems. *Int. J. Quantum Chem.* **2014**, *114*, 14–49.
- (56) Blöchl, P. E. Projector augmented-wave method. *Phys. Rev. B* **1994**, *50*, 17953–17979.
- (57) Kresse, G.; Joubert, D. From ultrasoft pseudopotentials to the projector augmented-wave method. *Phys. Rev. B* **1999**, *59*, 1758–1775.